# Three-dimensional fruit growth analysis clarifies developmental mechanisms underlying complex shape diversity in persimmon fruit

Akane Kusumi, Soichiro Nishiyama, Ryutaro Tao

Graduate School of Agriculture, Kyoto University, Sakyo-ku, Kyoto 606-8502, Japan

Correspondence: Soichiro Nishiyama (e-mail: nishiyama.soichiro.8e@kyoto-u.ac.jp, TEL: +81-75-753-6051)

**Abstract**

How fruit size and shape are determined is of research interest in agriculture and developmental biology. Fruit typically exhibits three-dimensional structures with genotype-dependent geometric features. Although minor developmental variations have been recognized, little research has fully visualized and measured these variations throughout fruit growth. In this study, a high-resolution 3D scanner was used to investigate the fruit development of 51 persimmon (*Diospyros kaki*) cultivars with various complex shapes. We obtained 2,380 3D fruit models that fully represented fruit appearance, and enabled precise and automated measurements of unique geometric features throughout fruit development. The 3D fruit model analysis identified key stages that determined the shape attributes at maturity. Typically, genetic diversity in vertical groove development was found, and such grooves can be filled by tissue expansion in the carpal fusion zone during fruit development. Furthermore, transcriptome analysis of fruit tissues from groove/non-groove tissues revealed gene co-expression networks that were highly associated with groove depth variation. The presence of *YABBY* homologs was most closely associated with groove depth and indicated the possibility that this pathway is a key molecular contributor to vertical groove depth variation. These results demonstrate the validity of fruit 3D growth analysis, which is a powerful tool for identifying the developmental mechanisms of fruit shape variation and the molecular basis of this diversity.

**Keywords**: *Diospyros kaki*; fruit shape; phenotyping; 3D measurement; *YABBY*

## Introduction

Fruit is an organ of angiosperms that facilitates reproduction. Generally, the fruit ovary protects seeds until they mature and promotes seed dispersal once fruit has reached maturity by color or aroma to attract animals (Howe and Smallwood, 1982). Fruits are classified by three characteristics: dehiscence or indehiscence, dry or fleshy, and unfused or fused carpels (Seymour et al. 2013). Fruit with fused carpels evolved from organs that are homologous to leaves (Scutt et al., 2006). Many studies demonstrated that mutations of genes related to floral development resulted in conversion of flowers into leaves, and that ectopic expression of those genes could transform leaves into floral organs and vice versa (Ferrándiz et al., 2010; Honma and Goto, 2001). After floral organ development is completed, fertilization stimulates hormonal and genetic change in ovules and ovaries; thus, fruit development is triggered (Mezzetti et al., 2004; Eklund et al., 2010). Fleshy fruit development is typically driven by cell division at the early stage and subsequently there is cell expansion (Gillaspy et al., 1993). Several major genes have been identified as affecting the final fruit size or shape by regulating the speed and direction of cell division and expansion (van der Knaap et al., 2014).

Fruit shape is an important agricultural trait and has been targeted in breeding (Cliff et al., 2002). In agricultural research practices, fruit shape has been evaluated by descriptive rating scales or 2D imaging of fruit. In particular, 2D imaging has been used for many species with various fruit shapes, such as tomato, cucumber, apple, and litchi (Gonzalo et al., 2009; Shimomura et al., 2016; Currie et al., 2000; Osako et al., 2020). In most cases, 2D imaging methods acquire images from one side of the fruit or from a sliced cross section, and shape features are obtained by image processing. Although 2D imaging-based quantitative evaluation of fruit shape is advantageous because the data collection can be quick, inexpensive, and simple, there are also disadvantages. Ding et al. (2000) found that the biggest disadvantage of 2D fruit morphology evaluation is that there is missing or reduced information. Two-dimensional evaluation often fails to capture part of the shape features that the original 3D structure possesses in that it represents only a single side of fruit and thus important information can be obscured. For this reason, 3D plant phenotyping has emerged and been applied in some important crops such as potato and strawberry (Liu et al., 2021; He et al., 2017; Li et al., 2020). Recent advances in photogrammetry have facilitated 3D image acquisition, yet very few studies have employed this technology to assess genetic diversity in fruit development.

Cultivated oriental persimmon (*Diospyros kaki* Thunb.), a temperate deciduous fruit tree, shows unique genetic variations in fruit development and shape (Nishiyama and Yamane, 2022). Regarding overall shape, some are flat, such as 'Hiratanenashi,' but others are elongated, such as 'Fudegaki.' In addition, some cultivars develop vertical and horizontal grooves ("Mizo" and "Za" in Japanese) in the lateral side and calyx end of the fruit, respectively, adding unique diversity to persimmon fruit shape (Fig. 1a and 1b). Conventionally, persimmon fruit shape diversity has been categorized into phenotype classes (Fruit Tree Experiment Station of Hiroshima Prefecture, 1979). For example, vertical groove depth was evaluated using a score and descriptor, such as "7. deep," "3. shallow, but obvious," or "1. absent." Similarly, horizontal grooves were evaluated as "9. extremely big," "3. small," or "1. absent." However, this qualitative categorization can produce confusion. In Fig. 1a, 'Mizushimagosho' and 'Amayotsumizo' were classified as having vertical grooves at the same level, though the actual depths are quite different. Therefore, developing a quantitative measurement method for persimmon fruit is beneficial in both agriculture and fruit development research.

Maeda et al. (2018) phenotyped persimmon fruit by chronologically applying an elliptic Fourier descriptors-based PCA method for 2D images of 153 *D. kaki* cultivars and two related species. The 2D imaging method successfully represented the ratio of length to diameter and the fruit apex shape, whereas components representing vertical and horizontal grooves were not detected. In fact, when the entire fruit is photographed from one direction, as in Maeda et al. (2018), the grooves in persimmon fruit are often self-occluded (Fig. 1c); thus, measurement by 2D-based methods is difficult. Ding et al. (2000) developed a 3D morphological analysis method for persimmon fruit. They captured the whole fruit contours using a CCD laser sensor system; however, there were few data points, and development of the unique persimmon fruit characteristics, such as horizontal and vertical grooves, have not yet been fully evaluated.

We previously showed potential applicability of photogrammetry-based 3D phenotyping of groove depths in persimmon fruit; shape measurements by geometric processing of the obtained 3D models represented the genetic diversity in the pattern of vertical groove depth (Kusumi et al., 2022). In this study, we applied a high-resolution 3D scanner to model the full growth of persimmon fruits with diverse shapes and to obtain regulatory information regarding fruit morphological development. In addition, transcriptome analysis was conducted to characterize the

molecular mechanism of vertical groove regulation.

## Materials and Methods

*Plant materials*

Fruit shapes were assessed for 51 *D. kaki* cultivars planted in the Kyoto Farmstead of the Experimental Farm of Kyoto University (Kyoto, Japan) (Table 1). Four to six fruits were sampled from each cultivar every 2 weeks, starting from the flowering stage in mid-May until the end of growth stage 1 in mid-August, and every 4 weeks after that until maturity, which varied among cultivars from the end of September to the beginning of November. However, due to the rottenness during the storage, 'Mizushimagosho' of 16 weeks after blooming (WAB) contained only 2 fruits. The persimmon development follows a double-sigmoid curve and growth stage 1 corresponds to the period when fruit development is drastically driven by active cell division and cell expansion (Nii, 1980).

*Acquiring 3D models*

A 3D Scanner Coordinate Measuring Machine (VL-500; KEYENCE, Osaka, Japan) was used to develop 3D models of the persimmon fruit. Fruit was sampled with the peduncle at the first 2 sampling periods, which were 0 and 2 WAB, and the fruit was scanned with the peduncle. After 4 WAB, the fruit calyx was removed to scan the precise features around it. Each persimmon fruit was set on a rotating table, and 3D images were obtained every 30 or 60 degrees; the interval at which images were taken (30 or 60 degrees) was based on sample complexity. The turning angle was optimized according to the fruit shape complexity, and image acquisition was iterated until a high-quality 3D model was obtained. This step was done for both side of each fruit, i.e., the calyx end and fruit apex, which led to an intact fruit 3D model when they were fused (Fig. 1c). The final model was saved as an STL file. All 3D models developed in this study is available at https://doi.org/10.6084/m9.figshare.22001908.

*Image processing*

MeshLab version 2021.05 (Cignoni et al., 2008), trimesh version 3.17.1

(https://github.com/mikedh/trimesh), and OpenCV version 3.1.0 (Bradski, 2000) were used to process 3D models and measure shape features, and the code is available at https://github.com/pomology-ku/persimmon-fruit-3D-measurement. Regarding the samples from 0 and 2 WAB, peduncles were manually removed using MeshLab. For all fruit models, the Z-axis was aligned to the calyx-apex line. Horizontal sections in the XY-plane were obtained by dividing the fruit model into 100 equal parts along the Z-axis. Additionally, 30 vertical sections were acquired by slicing the model by every 6° from the centroid origin.

Based on horizontal sections, vertical groove and roundness parameters were measured (Fig. 2a and Supplementary Fig. 1a). A parameter that represented vertical groove depth, Groove Index (GI), and Roundness (Ro) were calculated by the following equations:

$$Groove\ Index\ (GI) = \frac{Area\ of\ convexity\ defect}{Area\ of\ horizontal\ section}$$

$$Roundness\ (Ro) = \frac{Diameter\ of\ maximum\ inscribed\ circle\ of\ contour}{Diameter\ of\ minimum\ circumscribed\ circle\ of\ contour}$$

Length to width (L/W) ratio and horizontal grooves were evaluated from transverse sections. L/W ratio was calculated by the average of L/W from 30 sections (Fig. 3a). After detecting horizontal grooves based on curvature change, groove location was identified as the angle between the calyx–apex line and the line connecting the origin and detected groove. Groove location was averaged across 30 sections for each sample. It should be noted that horizontal groove measurement was conducted for eight cultivars with visible horizontal grooves (Table 1).

Finally, Tukey–Kramer's multiple comparison test ($p < 0.05$) was performed among different developmental stages to determine when these morphological parameters were fixed. The stage when the shape parameter score had no significant difference from mature fruit was considered the stage at which shape attributes were determined.

*Microscopic observation*

132 Five fruits from each of four cultivars (‘Mizuhimagosho,’ ‘Saijou,’ ‘Amayotsumizo,’ and ‘Fuyuu’), which
133 exhibited various GI at blooming, were sampled at anthesis in mid-May 2022. They were then fixed in the fixative
134 FAA (formalin: acetic acid: ethanol: distilled water = 2:1:10:7 v/v/v/v), followed by dehydration in a graded ethanol
135 series. Samples were cryo-embedded in blocks and cut into 6- or 8-µm-thick sections according to Kawamoto (1990).
136 Sections stained with toluidine blue were observed with an optical microscope (BX53FL, OLYMPUS, Tokyo, Japan).
137 Cell numbers and sizes were calculated as follows: first, baselines connecting the tips of seeds inside a fruit
138 were drawn (Fig. 4d). Second, line G (grooved zone) or N (non-grooved zone) was set from baseline to the point at
139 the contour of the fruit where the groove was deepest, or the point where the distance to the baseline was the longest.
140 Finally, number and size of cells that overlap with line G or N were measured. Parenchyma and tannin cells were
141 independently measured (Fig. 4e). To reduce the effect of outliers on cell size, the upper and lower 5% of data were
142 removed, and mean was calculated with the other 90% of the data. Wilcoxon rank sum test was conducted to assess
143 if there was significant difference between groove-present and -absent zones.
144
145 *Transcriptome analysis*
146 Fruits were sampled from eight cultivars (‘Zenjimaru,’ ‘Fuyuu,’ ‘Amayotsumizo,’ ‘Fujiwaragosho,’
147 ‘Gionbou,’ ‘Saijou,’ ‘Iwasedo,’ and ‘Mizushimagosho’) at 4 WAB (10 June 2022). Those cultivars were selected
148 because the vertical groove depth plateaus at around or after 4 WAB (except ‘Zenjimaru,’ which reached plateaus at
149 around 2 WAB). The grooved and non-grooved zones for each sample (Fig. 5a) were cut from each fruit, and the peel
150 and developing seeds were removed. Each tissue from each fruit was considered a single biological replicate, and
151 four or five fruits (replicates) were prepared for each cultivar and tissue type.
152 Total RNA was extracted by the hot borate method (Wan and Wilkins, 1994). Extracted RNA was quantified
153 using a Qubit 4 fluorometer (Invitrogen, Carlsbad, CA, USA). In total, 500 ng of total RNA was used to prepare
154 mRNAseq libraries. mRNAseq libraries were prepared using the NEBNext® Poly(A) mRNA Magnetic Isolation
155 Module, NEBNext® Ultra™ II RNA Library Prep Kit for Illumina®, and NEBNext® Multiplex Oligos for Illumina®
156 (New England Biolabs, Ipswich, MA, USA) following the manufacturer’s recommendations. The 78 libraries were
157 split into two groups of 40 and 38 to avoid barcode sequence overlap, and they were sequenced in one lane of

158 DNBSEQ (PE150) for each pool at Azenta Inc, Japan (Tokyo, Japan). All RNA samples used for RNAseq analysis
159 are listed in Supplementary Table 1. All sequence data are available in the DDBJ Sequenced Read Archive (accession
160 number DRA015493).

161 All sequences were pre-processed using fastp (Chen et al., 2018) with a minimum read length threshold of
162 35 bp. The reads from each library were aligned to the *Diospyros oleifera* reference genome (Suo et al., 2020) using
163 STAR with default parameters (Dobin, et al., 2013). Alignments were sorted using SAMtools (Li et al., 2009), and
164 the number of reads mapped to each contig was counted from the BAM files using HTseq-count (Putri et al., 2022).
165 Gene expression level was represented as transcripts per million (TPM).

166 Differential expression between grooved and non-grooved zones in groove-present cultivars was evaluated
167 using Deseq2 version 1.34.0 (Love et al., 2014) with the cultivar factor being input as cofactor of the model. A false
168 discovery rate of 0.05 was set to define differentially expressed genes (DEGs). Genes in the *D. oleifera* reference
169 genome was functionally annotated using eggNOG 5.0 (Huerta-Cepas et al., 2019) with default parameters. Gene
170 ontology enrichment analysis of the groove-associated DEGs was conducted using goseq (Young et al., 2010) with a
171 false discovery rate of 0.1 as the significance threshold. A gene co-expression network was constructed using
172 WGCNA (Langfelder and Horvath, 2008) with a TPM matrix for genes with TPM > 1 and the following parameters:
173 minModuleSize = 30, mergeCutHeight = 0.25. Soft thresholding power was set to 9, with a scale-free topology fitting
174 index of $R^2 > 0.85$. The gene module containing the *YABBY* homologs and network edges with topological overlap
175 greater than 0.30 was visualized using R package visNetwork version 2.1.2 (https://github.com/datastorm-
176 open/visNetworkg).

177

178

179 **Results**

180 *Three-dimensional modeling of persimmon fruit*

181 The VL-500 3D scanner developed fruit 3D models that precisely reflected morphological features of
182 persimmon fruit, including horizontal and vertical grooves (Fig. 1c, d). The polygon meshes of fruit 3D models
183 included at least 120 vertices per $mm^2$, which is sufficiently fine to evaluate fruit shape at flowering (*ca.* 4.08 mm in

184 longitudinal diameter) in the cultivar with the smallest ovary at flowering, 'Totsutanenashi.' Examples of horizontal
185 sections from 'Ooniwa' and 'Saijou' are shown in Fig. 1d. The slice contours showed clear grooves, and the models
186 included genetic differences in groove depth, including in 'Ooniwa,' which has deeper grooves and a deeper cavity
187 at the grooved zone. These general features of 3D models supported the feasibility of evaluating complex shape
188 attributes based on cross sections of the 3D models.
189
190 *Characterization of vertical groove development using 3D modeling*
191 To acquire a reliable metric to measure the shape attributes, GI and Ro were visualized over cross sections
192 from apex to calyx (Fig. 2a and Supplementary Fig. 1a). The contours in horizontal sections near the calyx or apex
193 were often rough and not stable because of concavity at the calyx and apex (Fig. 2b and Supplementary Fig. 1b).
194 Thus, GI and Ro were only evaluated from section #20-89, and were named GI#20-89 and Ro#20-89, respectively.
195 Fig. 2c represents the chronological change in GI#20-89 from all cultivars as clustered by Euclidean
196 distance. The cultivars with vertical grooves clustered in conventional categories but were largely separated into two
197 groups according to developmental pattern. We observed that all analyzed cultivars had vertical grooves in fruit at
198 flowering, and GI#20-89 decreased as fruit developed. By 6 WAB at the latest, the groove shape of 47/51 analyzed
199 cultivars showed GI#20-89 values consistent with the value at maturity, with the remaining four cultivars determined
200 at 8 WAB (Table 1). Therefore, vertical groove development was mainly determined in the initial stage of fruit
201 development, at which time active cell division rather than cell expansion takes place.
202
203 *Roundness and its association with vertical groove depth*
204 Roundness was also evaluated from transverse sections. Supplementary Fig. 1 shows a chronological
205 change in Ro#20-89 for all cultivars, as classified by Euclidean distance. Generally, Ro#20-89 tended to increase
206 with development, which indicated that the fruit became round during development. Interestingly, cultivars with
207 vertical grooves generally clustered together; these cultivars tended to be less round. In contrast to vertical grooves,
208 roundness-determining periods were more variable among cultivars, and roundness was mainly formed by 10 WAB
209 (Table 1).

To further investigate the relationship between the groove depth and roundness, Spearman's rank correlation analysis was performed. Through developmental stages, groove depth and roundness were significantly correlated with each other ($p < 0.01$) (Supplementary Fig. 2a), which indicated that grooved fruit tends to be square-shaped. At 0 WAB, the correlation coefficient was −0.518. Then, the coefficient gradually increased and reached −0.743 at maturity (Supplementary Fig. 2b).

*Horizontal groove and L/W development during fruit growth*

Horizontal grooves and L/W development were evaluated using 30 vertical sections of each fruit (Fig. 3a). Supplementary Fig. 3a shows a chronological change in L/W for all cultivars, as classified by Euclidean distance. L/W remained low through the development of flat cultivars; however, it increased toward maturity in oblong cultivars. 'Fudegaki' and 'Nagara,' which have oblong fruit, exhibited drastic changes in L/W. L/W was determined within the first developmental stage in most cultivars, but there were several cultivars whose L/W was not determined by 24 WAB. Cultivars with late determination included many oblong cultivars, such as 'Nagara,' 'Fudegaki,' 'Saijou,' and 'Aburatsubo.'

Detecting horizontal grooves was difficult and produced many missing values. This is because the grooves typically did not cover the entire fruit, or the curvature change at the grooves in vertical sections were not as large as other depressions in fruits (Fig. 3b). Additionally, horizontal grooves at the fruit calyx may be missing from the samples harvested at 0 and 2 WAB because those samples had peduncles when scanned. Fig. 3c shows the chronological change in horizontal groove point angles, which represented the location of horizontal grooves, for fruit from eight cultivars, as classified by Euclidean distance. Generally, the score increased as fruit grew, which indicated that horizontal grooves tended to move from the calyx to apex. In particular, 'Tamopan,' which has an "extremely big" horizontal groove (Fruit Tree Experiment Station of Hiroshima Prefecture, 1979), had a distinctive pattern of groove development; the grooved zone kept moving toward the apex throughout fruit development. However, 'Kikuhira' and 'Mizushimagosho' did not show any significant differences in groove position from horizontal groove emergence. Groove development became stable at 10 WAB in 'Tenpougai,' 'Midai,' 'Nagara,' and 'Fudegaki,' and at 12 WAB in 'Sakata' (Supplementary Fig. 5).

236 We determined that changes in the horizontal groove position can be inferred by vertical growth speed of
237 the calyx and apex portions, which were separated by the horizontal groove; the groove moved toward the apex when
238 the growth speed of the calyx above the horizontal groove was faster than that of the apex beneath the groove. This
239 pattern was observed in the models of cultivars with large horizontal grooves. Additionally, horizontal groove depth
240 can be inferred by horizontal growth speed of these portions. In 'Tenpougai' and 'Tamopan,' the groove depth
241 continued to increase from anthesis, but the increase suspended at mid-growth and showed double-sigmoid curve
242 patterns (Fig. 3d). Fruit volume analysis in 'Tamopan' showed that the apex, which was beneath the groove, exhibited
243 a double sigmoid-like curve, but the calyx, which was above the groove, did not follow this pattern and continued to
244 develop (Fig. 3e). In addition, the volume increase ratio was larger in the calyx than in the apex throughout the
245 developmental stages except at 20 WAB. Especially in the early growing period, the differences were much larger
246 (Fig. 3e). Taken together, horizontal groove movement was explained by a developmental model in which the
247 horizontal and vertical growth speeds of the calyx were faster than those of the apex during growth stage 1, but
248 became similar around stages 2–3 depending on cultivar (Fig. 3f).
249
250 *Developmental analysis of vertical groove variation*
251 We conducted an in-depth analysis of the genetic diversity of vertical grooves that many cultivars possess.
252 Persimmon generally have four carpels, and vertical grooves develop at carpel fusion zones (Fig. 4a). Most
253 persimmon cultivars show various degrees of a vertical groove at anthesis, regardless of vertical groove presence or
254 absence at maturity (Fig. 2c). However, the groove depth can become shallower during development depending on
255 genotype (Fig. 4b). Considering the groove development pattern along with persimmon fruit enlargement, we
256 hypothesized that groove depth is primarily determined by cell division. Thus, groove development for ovarian tissues
257 was characterized before and at anthesis in four cultivars with various groove depths.
258 At approximately 3 weeks before anthesis, groove lines were visible along the carpel fusion lines in
259 'Amayotsumizo' and 'Mizushimagosho,' but not in 'Fuyuu' (Fig. 4c). Microscopy revealed no significant difference
260 between cell sizes in groove-present and -absent zones regardless of the cell types and cultivars, but there was a
261 significant increase in all cells (tannin cells and parenchyma cells) and parenchyma cells detected in groove-absent

262 tissue compared with groove-present tissue (Fig. 4d, 4e, 4f and Supplementary Fig. 4, $p < 0.05$). For tannin cell
263 number, a significant difference was only observed in 'Saijou.' Based on those results, we suggest that vertical groove
264 formation at anthesis is driven by the variations in cell layers of fruit flesh, mainly of parenchyma tissues.

265 We further characterized molecular genetic regulation of vertical groove development using a
266 transcriptomic approach. In differential expression analysis, genetic variation was categorically incorporated into the
267 multi-factor model to standardize differences in genetic background among cultivars. The differential expression
268 analysis identified 1,883 DEGs between grooved and non-grooved zones in groove-present cultivars. DEGs were
269 typically enriched for functions in cell wall development and cell fate determination (Table 2). To search for candidate
270 regulators, we identified the lowest q-values, which yielded genes with typical functions in fruit development, such
271 as cell wall-related genes and well-characterized transcription factors (Table 3). Specifically, *SVP* and *YABBY*
272 homologs were among the top 20 DEGs with the lowest q-values (Table 3).

273 *SVP* is a MADS-box factor that determines floral meristem identity (Gregis et al., 2008). The diploid
274 *Diospyros* reference genome has two *SVP* homologs (Supplementary Fig. 6). One *SVP* homolog
275 (evm.model.original_scaffold_495.37), *DkSVP1*, was the DEG with the second lowest q-value among all genes and
276 showed lower expression in groove than non-groove tissue in groove-present cultivars (Supplementary Fig. 6). The
277 same expression pattern was found in groove-absent cultivars. Interestingly, the other *SVP* homolog, *DkSVP2*
278 (evm.model.original_scaffold_1207.202), generally showed opposite expression compared with *DkSVP1*: there was
279 higher expression in groove than in non-groove tissues.

280 The *YABBY* gene family is a central regulator of carpel development. In *Arabidopsis*, *YAB1* and *YAB3* are
281 known to have roles in carpel fusion development (Nole-Wilson and Krizek, 2006). The DEGs highly associated with
282 groove development, evm.model.original_scaffold_883.29 and evm.model.original_scaffold_1133.35 (*DkYABBY1a*
283 and *DkYABBY1c*, respectively), were found in the YAB1/YAB3 clade (Supplementary Fig. 7). *DkYABBY1a* and
284 *DkYABBY1c* expression patterns matched the patterns of groove development and genetic variation. They were
285 significantly more expressed in the grooved zone in groove-present cultivars, and the expression level was higher in
286 cultivars with deeper vertical grooves; however, there were no significant differences between tissues in the groove-
287 absent cultivars (Fig 5c). Similar expression patterns were also observed in evm.model.fragScaff_scaffold_45.107

288 (*DkYABBY5a*) and evm.model.original_scaffold_1639.203.1 (*DkYABBY1b*) (Supplementary Fig. 7).

289 The functions and expression patterns of *YABBY* family genes explained the groove depth variation.
290 Therefore, we further characterized the associated gene networks (Fig. 5d and Supplementary Fig. 8). Genes with
291 first-degree interactions with *YABBY* genes did not include transcription factors. However, many transporter genes
292 and enzyme-coding genes were found, such as *CYP77A4*, which functions in auxin-mediated patterning (Kawade et
293 al., 2018), and *CYP86A8*, which functions in omega-hydroxylation of various fatty acids during development
294 (Wellesen et al., 2008). Collectively, these results identify the *YABBY* family as a potential molecular factor that
295 directly regulates vertical groove development.

296

297

298 **Discussion**

299 *Utilizing 3D scan for geometric phenotyping of fruit*

300 This study showed that 3D models developed by a 3D scanner captured detailed morphological features of
301 persimmon fruit. In particular, fine characteristics of complex features, such as horizontal and vertical grooves, were
302 clearly reproduced (Fig. 1c and 3b). Conventional persimmon fruit phenotyping was previously conducted based on
303 2D imaging (Maeda et al., 2018, 2019; Kusumi et al., 2022), which did not capture all shape attribute information.
304 In this study, we obtained morphological information along various axes. For example, vertical grooves are more
305 prominent near the calyx or apex in some cultivars, but they are more noticeable in the middle portion of the fruit in
306 other cultivars. However, 2D imaging cannot capture grooves that form near the apex because it is obscured when
307 imaged from one side of the fruit. In addition, the horizontal grooves do not typically cover the entire fruit
308 circumference, which results in loss of information when conducting 2D imaging. To address these issues, we used a
309 3D modeling approach that allowed us to integrate information from multiple sections along the calyx–apex line.

310

311 *3D modeling clarifies complex shape development in persimmon fruit*

312 In this study, we observed that the vertical groove depth decreased during growth stage 1, with variations
313 depending on genotype. However, all cultivars had vertical grooves at anthesis, but with differing depths (Figs. 2 and

314 4). These results indicate that groove formation was influenced by both carpel fusion and cell growth patterns at the
315 carpel margin. The numbers of cell layers, but not cell size, were significantly higher in the groove-present area,
316 which indicated that the cell layer difference may be the main factor that influences groove formation. Interestingly,
317 vertical groove depth was negatively correlated with roundness. The correlation coefficients continued to decrease
318 and reached $r = -0.743$ at maturity (Supplementary Fig. 2); this indicated a common mechanism underlying both
319 vertical groove depth and roundness, and is most likely associated with carpel fusion pattern.

320 We concluded that the horizontal groove development in persimmon fruit is promoted by the different
321 growth speeds between fruit portions above and beneath the groove. In this study, we observed that the horizontal
322 groove moved toward the apex and the groove continued to deepen throughout fruit development (Fig. 3c and 3d).
323 This demonstrates that both vertical and horizontal development speeds, which correspond to groove position and
324 groove depth, respectively, of calyx tissues above the groove were much faster than those of the apex during early
325 fruit growth, and became similar later (Fig. 3e). These observations are consistent with the findings of previous
326 studies, which reported that growth at the calyx in persimmon fruit is more vigorous during stage 1, which could
327 continue until early-mid August (Fujimura, 1935). Collectively, we showed that differences in the horizontal and
328 vertical growth speeds between portions of the fruit, divided by the horizontal groove, explained horizontal groove
329 development and movement (Fig. 3f).

330 Maeda et al. (2018) reported that fruit L/W ratio was the main contributor to shape variation in longitudinal
331 fruit sections based on PCA of diverse persimmon cultivars. They found that the correlation coefficients between
332 PC1, which represented L/W ratio variability, at maturity and that of several different developmental stages reached
333 0.9 at the end of June. In this experiment, correlation analysis was conducted between the L/W ratio at maturity and
334 that of different developmental stages. The correlation coefficient reached at 0.9 between 4–6 WAB (Supplementary
335 Fig. 3b). This result was also consistent with that of Sugiura et al. (1977), in which ethanol treatment of persimmon
336 fruits after flowering until late July influenced the fruit L/W ratio. In this study, we further showed that each genotype
337 had variable transitions; the period for determining L/W ratio varied from 0 WAB to maturity depending on cultivar
338 (Table 1). In addition, we found that the L/W ratio was determined later in cultivars with oblong fruit, such as
339 'Fudegaki' or 'Nagara.' This probably means that vertical cell division or expansion receive more resources in oblong

340 cultivars, which causes slower transverse development, but horizontal and vertical development can become equal
341 earlier in other cultivars.
342
343 *Cell identity control is the most likely mechanism underlying vertical groove development variation*
344 Vertical grooves in fruit are known to emerge in many species, including *Cucumis* and *Prunus* (Paris, 2016;
345 Yousif et al., 2011). Multiple genetic studies have explored the genes that contribute to groove formation, but the
346 molecular mechanism of their development is not fully understood. Yao et al. (2018) found that overexpression of
347 *Malus domestica PISTILLATA* causes vertical groove development on fruit from 12 days after pollination. Du et al.
348 (2022) identified a 1.07-kb deletion of a chromosome segment in groove lines of *Cucumis melo* and proposed that
349 *CmMADS-Box* may be a candidate gene regulating the groove formation. It was also reported that certain *Arabidopsis*
350 mutants with defects in the *YABBY* and *SVP* genes produced flowers with abnormal carpel fusions, which can possibly
351 lead to groove-like structures (Nole-Wilson and Krizek, 2006; Gregis et al., 2009). However, there has been no report
352 to date of *YABBY* or *SVP* directly regulating groove formation in species with fleshy fruit.
353 Our transcriptome analysis indicated that DEGs between grooved and non-grooved zones were related to
354 cell wall development or cell fate, which is consistent with the observation that grooves were formed by fewer cell
355 layers at carpel margins (Fig. 4). Interestingly, of the DEGs, *SVP* and *YABBY* gene families had low q-values (Table
356 2). *SVP* is known to be involved in determination of floral organ identity in *Arabidopsis* and tomato (Liu et al., 2007;
357 Thouet et al., 2012). However, *YABBY* controls establishment of abaxial–adaxial polarity in lateral organs (van der
358 Knapp et al., 2014). *YABBY* is a plant-specific transcription factor with several family members (Bowman, 2000);
359 *FIL/YAB3* define the abaxial cell fate in lateral organs in *Arabidopsis* (Siegfried et al., 1999), whereas *FASCINATED*
360 (homologous to *YAB2*) in tomato has been reported to control carpel number (Cong et al., 2008). Importantly, *DkSVP1*
361 expression was also high in groove-absent cultivars, whereas *DkYABBY1a* and *DkYABBY1c* expression completely
362 matched the groove patterns, including presence/absence among different cultivars (Fig 5c). These results strongly
363 suggest that *YABBY* homologs are direct regulators of vertical groove development.
364 The gene co-expression network of *DkYABBY1a/1c* did not include any transcription factors, which
365 indicated that *YABBY*s are upstream regulators of the network (Fig. 5d). Most genes associated with *YABBY*s are

366 transporters and enzymes, and they seemed to be functionally related to cell development. In particular, enzymes
367 related to hydrocarbon metabolism were highly enriched, such as cytochrome P450 proteins (Fukushima et al., 2011)
368 and lipolytic enzymes. *CYP77A4* was reported to be involved in establishing polarity in *A. thaliana* embryos by
369 regulating auxin distribution pattern; thus, it plays an important role in leaf morphogenesis (Kawade et al., 2018).
370 Additionally, pectate lyase was found in the network, which helps cell wall remodeling (Uluisik and Seymour, 2020).
371 Considering the expression pattern, biological function in model species, and co-expression network, it is very likely
372 that the *YABBY* homologs directly regulate vertical groove development. It should be noted that multiple *YABBY*
373 homologs were expressed in a highly correlated manner, which indicates an additional layer of expression regulation
374 underlying the genetic variation in vertical groove development. Further functional analysis, including examination
375 of characteristic paralogs, in persimmon may offer new insights into this process.
376
377
378 **Acknowledgments**
379 We thank Mallory Eckstut, PhD, from Edanz (https://jp.edanz.com/ac) for editing a draft of this manuscript.
380 This work was supported by the Japan Society for the Promotion of Science KAKENHI Grant Number 20K20454 to
381 SN and RT, and 21KK0269 to SN.
382
383 **References**
384 Bowman, J.L. 2000. The *YABBY* gene family and abaxial cell fate. Curr. Opin. Plant Biol. 3：17-22.
385 Bradski, G. 2000. The OpenCV Library. Dr. Dobb's j. softw. tools prof. program. 25: 120-123.
386 Chen, S., Y. Zhou, Y. Chen and J. Gu. 2018. Fastp: An ultra-fast all-in-one FASTQ preprocessor. Bioinformatics. 34:
387 i884–i890.
388 Cignoni, P., M. Callieri, M. Corsini, M. Dellepiane, F. Ganovelli and G. Ranzuglia. 2008. MeshLab: an Open-Source
389 Mesh Processing Tool. Sixth Eurographics Italian Chapter Conference.129-136
390 Cliff, M., K. Sanford, W. Wismer and C. Hampson. 2002. Use of digital images for evaluation of factors responsible
391 for visual preference of apples by consumers. HortScience. 37: 1127-1131

392 Cong, B., L.S. Barrero and S.D. Tanksley. 2008. Regulatory change in *YABBY*-like transcription factor led to
393 evolution of extreme fruit size during tomato domestication. Nat. Genet. 40:800–804.
394 Currie, A.J., S. Ganeshanandam, D.A. Noiton, D. Garrick, C.J.A. Shelbourne and N. Oraguzie. 2000. Quantitative
395 evaluation of apple (*Malus* × *domestica* Borkh.) fruit shape by principal component analysis of Fourier
396 descriptors, Euphytica. 111: 221-227
397 Ding, W., Nesumi, H., Yamada, M., Takano, Y., 2000. Quantitative evaluation of 3-dimentional fruit morphology and
398 its applications to genetic analysis. Jpn. J. Biomet. 20, 131-141, in Japanese with English abstract.
399 Dobin, A., C.A. Davis, F. Schlesinger, J. Drenkow, C. Zaleski, S. Jha, P. Batut, M. Chaisson and T.R. Gingeras. 2013.
400 STAR: Ultrafast universal RNA-seq aligner. Bioinformatics 29:15–21.
401 Du, X., H. Liu, Z. Zhu, S. Liu, Z. Song, L. Xia, J. Zhao, F. Luan and S. Liu. 2022. Identification of candidate
402 chromosome region related to melon (*Cucumis melo* l.) fruit surface groove trait through biparental genetic
403 mapping and genome-wide association study. Front. Plant Sci. 13.
404 Ferrándiz, C., C. Fourquin, N. Prunet, C.P. Scutt, E. Sundberg, C. Trehin, A. Lie and C.M. Vialette-Guiraud. 2010.
405 Carpel Development. Adv. Bot. Res. 55: 1-73
406 Fruit Tree Experiment Station of Hiroshima Prefecture. 1979. Showa 53-nendo Shubyo-tokusei-bunrui-chosa-
407 hokokusho (Kaki). Fruit Tree Experiment Station of Hiroshima Prefecture, Hiroshima, Japan. In Japanese.
408 Fujimura, J. 1935. The research on persimmon fruit development. J. Jpn. Soc. Hortic. Sci. 6: 105-117. In Japanese.
409 Fukushima, E.O., H. Seki, K. Ohyama, E. Ono, N. Umemoto, M. Mizutani, K. Saito and T. Muranaka. 2011.
410 *CYP716A* subfamily members are multifunctional oxidases in triterpenoid biosynthesis. Plant Cell Physiol.
411 52:2050–2061.
412 Gillaspy, G., H. Ben-David and W. Gruissem. 1993. Fruits: a developmental perspective, The Plant Cell. 5: 1439-
413 1451.
414 Gonzalo, M.J., M.T. Brewer, C. Anderson, D. Sullivan, S. Gray and E. van der Knaap. 2009. Tomato fruit shape
415 analysis using morphometric and morphology attributes implemented in Tomato Analyzer software program. J.
416 Am. Soc. Hortic. 134: 77-87
417 Gregis, V., A. Sessa, L. Colombo and M.M. Kater. 2008. *AGAMOUS-LIKE24* and *SHORT VEGETATIVE PHASE*

418 determine floral meristem identity in Arabidopsis. Plant Journal 56:891–902.

419 He, J.Q., R.J. Harrison and B. Li. 2017. A novel 3D imaging system for strawberry phenotyping. Plant Methods. 13.

420 Honma, T and K. Goto. 2001. Complexes of MADS-box proteins are sufficient to convert leaves into floral organs.
421 Nature. 409: 525–529

422 Howe, H.F. and J. Smallwood. 1982. Ecology of Seed Dispersal, Source: Annual Review of Ecology and Systematics.
423 13: 201-228

424 Huerta-Cepas, J., D. Szklarczyk, D. Heller, A. Hernández-Plaza, S.K. Forslund, H. Cook, D.R. Mende, I. Letunic, T.
425 Rattei, L.J. Jensen, C. von Mering and P. Bork. 2019. EggNOG 5.0: A hierarchical, functionally and
426 phylogenetically annotated orthology resource based on 5090 organisms and 2502 viruses. Nucleic Acids Res.
427 47: D309–D314.

428 Kawade, K., Y. Li, H. Koga, Y. Sawada, M. Okamoto, A. Kuwahara, H. Tsukaya and M.Y. Hirai. 2018. The
429 cytochrome P450 CYP77A4 is involved in auxin-mediated patterning of the Arabidopsis thaliana embryo.
430 Development. 145.

431 Kawamoto, T. 1990. Light microscopic autoradiography for study of early changes in the distribution of water-soluble
432 materials. J. Histochem. Cytochem. 38: 1805-1814.

433 van der Knaap, E., M. Chakrabarti, Y.H. Chu, J.P. Clevenger, E. Illa-Berenguer, Z. Huang, N. Keyhaninejad, Q. Mu,
434 L. Sun, Y. Wang and S. Wu. 2014. What lies beyond the eye: the molecular mechanisms regulating tomato fruit
435 weight and shape. Front. Plant Sci. 5:227

436 Kusumi, A., Y. Osako, R. Nakano, S. Nishiyama and R. Tao. 2022. Phenotypic evaluation of shape diversity in
437 persimmon fruit using two- and three-dimensional imaging. Acta Horticulturae. International Society for
438 Horticultural Science: 263-268.

439 Langfelder, P. and S. Horvath. 2008. WGCNA: An R package for weighted correlation network analysis. BMC
440 Bioinformatics 9.

441 Li, H., B. Handsaker, A. Wysoker, T. Fennell, J. Ruan, N. Homer, G. Marth, G. Abecasis and R. Durbin. 2009. The
442 sequence alignment/map format and SAMtools. Bioinformatics. 25: 2078-2079.

443 Li, M., M.R. Shao, D. Zeng, T. Ju, E.A. Kellogg and C.N. Topp. 2020. Comprehensive 3D phenotyping reveals

continuous morphological variation across genetically diverse sorghum inflorescences. New Phytol. 226: 1873-1885.

Liu, C., J. Zhou, K. Bracha-Drori, S. Yalovsky, T. Ito and H. Yu. 2007. Specification of *Arabidopsis* floral meristem identity by repression of flowering time genes. Development 134:1901–1910.

Liu, J., X. Xu, Y. Liu, Z. Rao, M.L. Smith, L. Jin and B. Li. 2021. Quantitative potato tuber phenotyping by 3D imaging. Biosyst. Eng. 210:48–59.

Love MI, W. Huber and S. Anders. 2014. Moderated estimation of fold change and dispersion for RNA-seq data with DESeq2. Genome Biol. 15: 550.

Maeda, H., T. Akagi and R. Tao. 2018. Quantitative characterization of fruit shape and its differentiation pattern in diverse persimmon (*Diospyros kaki*) cultivars. Sci. Hortic. 228:41–48.

Maeda, H., T. Akagi, N. Onoue, A. Kono, and R. Tao, Evolution of lineage-specific gene networks underlying the considerable fruit shape diversity in persimmon. Plant Cell Physiol. 60:2464–2477

Magnus Eklund, D., V. Ståldal, I. Valsecchi, I. Cierlik, C. Eriksson, K. Hiratsu, M. Ohme-Takagi, J.F. Sundström, M. Thelander, I. Ezcurra and E. Sundberg. 2010. The *Arabidopsis thaliana* STYLISH1 protein acts as a transcriptional activator regulating auxin biosynthesis. Plant Cell 22:349–363.

Mezzetti, B., L. Landi, T. Pandolfini and A. Spena. 2004. The *defH9-iaaM* auxin-synthesizing gene increases plant fecundity and fruit production in strawberry and raspberry BMC Biotechnol. 4:4.

Nii, N. 1980. Seasonal changes of fruit growth in Japanese persimmon, *Diospyros kaki* cv. Fuyu, in relation to vascular tissue development in the fruit stalk. J. Jpn. Soc. Hortic. Sci. 49: 160-170.

Nishiyama, S. and H. Yamane. 2022. Fruit-Size Control. In: The Persimmon Genome: Springer, Cham. p. 155–165.

Nole-Wilson, S. and B.A. Krizek. 2006. AINTEGUMENTA contributes to organ polarity and regulates growth of lateral organs in combination with YABBY genes. Plant Physiol. 141:977–987.

Onoue, N., S. Kobayashi, A. Kono and A. Sato. 2018. SSR-based molecular profiling of 237 persimmon (*Diospyros kaki* Thunb.) germplasms using an ASTRINGENCY-linked marker. Tree Genet. Genomes 14: 1-18.

Osako, Y., H. Yamane, S.Y. Lin, P.A. Chen and R. Tao. 2020. Cultivar discrimination of litchi fruit images using deep learning. Sci. Hortic. 269.

470 Paris, H.S. 2016. Germplasm enhancement of *Cucurbita pepo* (pumpkin, squash, gourd: Cucurbitaceae): progress
471 and challenges. Euphytica. 208: 415-438.
472 Putri, G.H., S. Anders, P.T. Pyl, J.E. Pimanda and F. Zanini. 2022. Analysing high-throughput sequencing data in
473 Python with HTSeq 2.0. Bioinformatics 38:2943–2945.
474 Scutt, C.P., M. Vinauger-Douard, C. Fourquin, C. Finet and C. Dumas. 2006. An evolutionary perspective on the
475 regulation of carpel development. J. Exp. Bot. 57: 2143-2152
476 Seymour, G.B., L. Ostergaard, N.H. Chapman, S. Knapp and C. Martin. 2013. Fruit development and ripening. Annu.
477 Rev. Plant Biol.
478 Shimomura, K., H. Horie, M. Sugiyama, Y. Kawazu and Y. Yoshioka. 2016. Quantitative evaluation of cucumber
479 fruit texture and shape traits reveals extensive diversity and differentiation. Sci. Hortic. 199:133–141.
480 Siegfried, K.R., Y. Eshed, S.F. Baum, D. Otsuga, G.N. Drews and J.L. Bowman. 1999. Members of the *YABBY* gene
481 family specify abaxial cell fate in *Arabidopsis*. Development. 126: 4117-4128.
482 Suo, Y., P. Sun, H. Cheng, W. Han, S. Diao, H. Li, Y. Mai, X. Zhao, F. Li and J. Fu. 2020. A high-quality chromosomal
483 genome assembly of *Diospyros oleifera* Cheng. Gigascience 9.
484 Sugiura, A., H. Harada and T. Tomana. 1977. Studies on the removal of astringency in Japanese persimmon fruits Ⅱ.
485 on-tree removal of astringency by ethanol treatment (Part II). J. Jpn. Soc. Hortic. Sci. 46: 303-309 in Japanese
486 with English abstract.
487 Thouet, J., M. Quinet, S. Lutts, J.M. Kinet and C. Périlleux. 2012. Repression of floral meristem fate is crucial in
488 shaping tomato inflorescence. PLoS One 7.
489 Uluisik, S. and G.B. Seymour. 2020. Pectate lyases: Their role in plants and importance in fruit ripening. Food Chem.
490 309: 125559.
491 Wan, C.Y. and T. A. Wilkins. 1994. A modified hot borate method significantly enhances the yield of high-quality
492 RNA from cotton (*Gossypium hirsutum* L.). Anal. Biochem. 223: 7-12.
493 Wellesen, K., F. Durst, F. Pinot, I. Benveniste, K. Nettesheim, E. Wisman, S. Steiner-Lange, H. Saedler and A.
494 Yephremov. 2001. Functional analysis of the *LACERATA* gene of *Arabidopsis* provides evidence for different
495 roles of fatty acid $\omega$-hydroxylation in development. Proc. Natl. Acad. Sci. U.S.A. 98:9694-9699.

496 Yao, J.L., J. Xu, S. Tomes, W. Cui, Z. Luo, C. Deng, H.S. Ireland, R.J. Schaffer and A.P. Gleave. 2018. Ectopic
497 expression of the *PISTILLATA* homologous *MdPI* inhibits fruit tissue growth and changes fruit shape in apple.
498 Plant Direct 2: e00051.
499 Young, M.D., M.J. Wakefield, G.K. Smyth and A. Oshlack. 2010. Gene ontology analysis for RNA-seq: accounting
500 for selection bias. Genome Biol. 11: 1-12.
501 Yousif, M.T., T.M. Elamin, A. Fadil, M. Baraka, A.A. el Jack and E.A. Ahmed. 2011. Variability and correlation
502 among morphological, vegetative, fruit and yield parameters of snake melon (*Cucumis Melo* Var. Flexuosus).
503 Cucurbit Genet. Coop. Report. 33: 32-35.
504

505 **Conflict of Interest**

506 The authors declare no conflict of interest.

507

508

509 **Figure legends**

510 **Figure 1. Three-dimensional scanning of fruit from diverse persimmon cultivars.** (a, b) Diversity of (a) vertical
511 and (b) horizontal grooves in persimmon fruits. (c) An example of self-occlusions in 'Gobangaki.' (d) 3D model of
512 'Ooniwa' at maturity. (e) Horizontal sections of 3D models. Scores and descriptors in (a) and (b) are based on Fruit
513 Tree Experiment Station of Hiroshima Prefecture (1979).

514 **Figure 2. Characterization of vertical groove development.** (a) Schematic of the measurement method used to
515 determine groove index (GI). (b) Transition of GI in 'Ooniwa' throughout developmental stages. (c) Heatmap of the
516 transition of GI#20-89, with asterisks indicating cultivars classified as having vertical grooves by Fruit Tree
517 Experiment Station of Hiroshima Prefecture (1979) and visually verified when no recorded reference was available.

518 **Figure 3. Characterization of horizontal groove development.** (a) Schematic of the measurement method used to
519 determine horizontal grooves. (b) 3D models of (i) 'Kikuhira,' (ii) 'Nagara,' (iii) 'Sakata,' (iv) 'Fudegaki,' (v)
520 'Tenpougai,' (vi) 'Tamopan,' (vii) 'Midai,' and (viii) 'Mizushimagosho.' (c) Heatmap of the transition of groove
521 position (angle between line A and line B in Figure 3a). (d) Transition patterns of groove depth in 'Tenpougai' and
522 'Tamopan.' The black line indicates the horizontal groove depth. (e) Transition of volume and volume increase ratio
523 in 'Tamopan.' (f) Proposed developmental model for horizontal grooves.

524 **Figure 4. Morphological characterization of groove tissue.** (a) 3D model of 'Gionbou' at anthesis showing grooves
525 at the boundaries of the fused carpels. (b) Chronological change of groove development in 'Gionbou.' (c) Ovaries of
526 (i) 'Amayotsumizo,' (ii) 'Mizushimagosho,' and (iii) 'Fuyuu' at three weeks before anthesis (23 April 2022).
527 Grooving lines were observed in (i) and (ii), but not in (iii). (d) Measurement of cell number and area in the grooved
528 and non-grooved zones using baselines set at the tip of developing seeds. (e) Microscopy analysis performed on
529 grooved and non-grooved zones for four cultivars. MIZ, SAI, AMA, and FUY represent 'Mizushimagosho,' 'Saijou,'
530 'Amayotsumizo,' and 'Fuyuu,' respectively. (f) Comparison of parenchyma cell size, tannin cell size, and cell layers
531 measured in each zone (grooved, G, and non-grooved, N) in four cultivars. Single and double asterisks indicate
532 significant differences at $p < 0.05$ and $p < 0.01$, respectively.

533 **Figure 5. Transcriptome analysis of vertical groove development.** (a) Grooved (G) and non-grooved (N) zones
534 from which RNA was extracted. (b) Vertical groove depths at 4 and 20 WAB. (c) Expression patterns of *DkYABBY1a*

535 and *DkYABBY1c*. (d) Gene co-expression network for *DkYABBY1a*/*1c*. The full network of this module is presented

536 in Supplementary Figure S8. ZEN, FUY, FUJ, IWA, GIO, MIZ, SAI, and AMA represent 'Zenjimaru,' 'Fuyuu,' 'Fuji,'

537 'Iwasedo,' 'Gionbou,' 'Mizushimagosho,' 'Saijou,' and 'Amayotsumizo,' respectively.

538

539

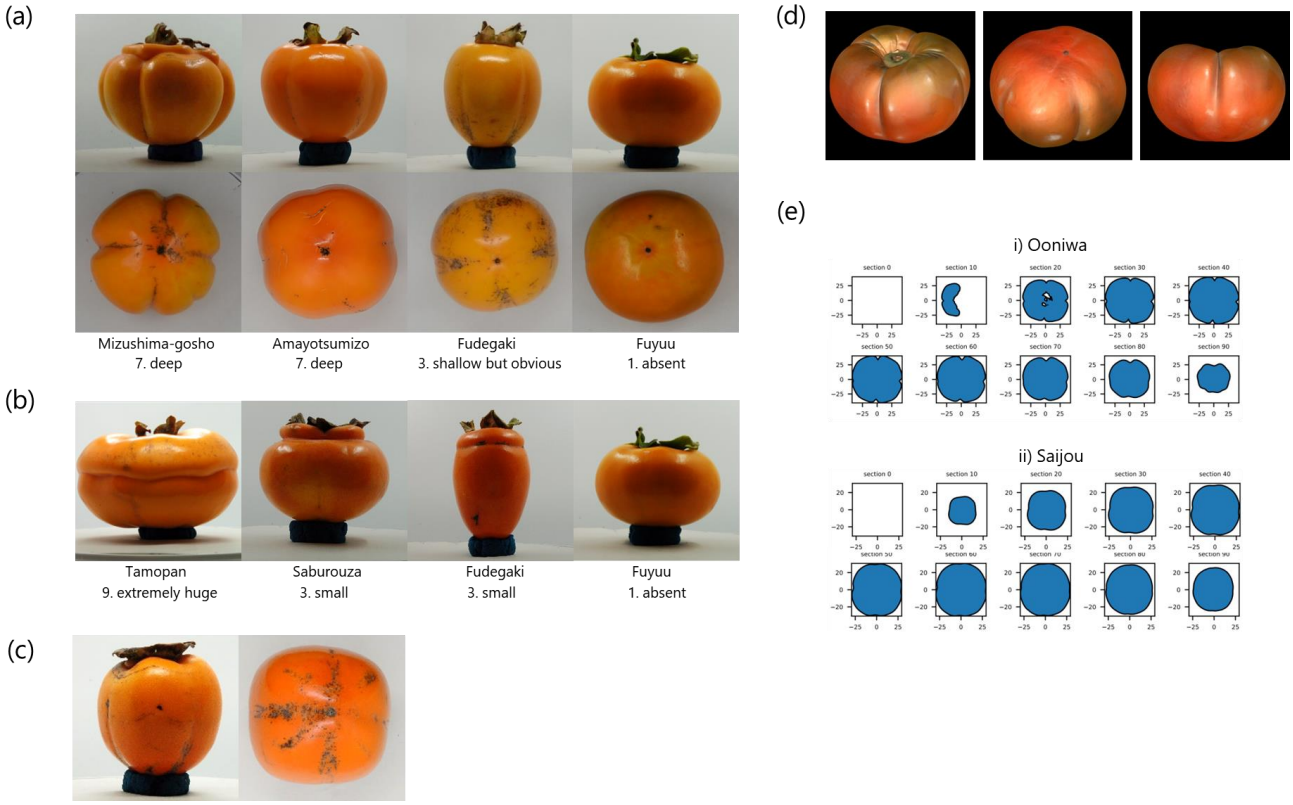


**Figure 1. Three-dimensional scanning of fruit from diverse persimmon cultivars.** (a, b) Diversity of (a) vertical and (b) horizontal grooves in persimmon fruits. (c) An example of self-occlusions in 'Gobangaki.' (d) 3D model of 'Ooniwa' at maturity. (e) Horizontal sections of 3D models. Scores and descriptors in (a) and (b) are based on Fruit Tree Experiment Station of Hiroshima Prefecture (1979).

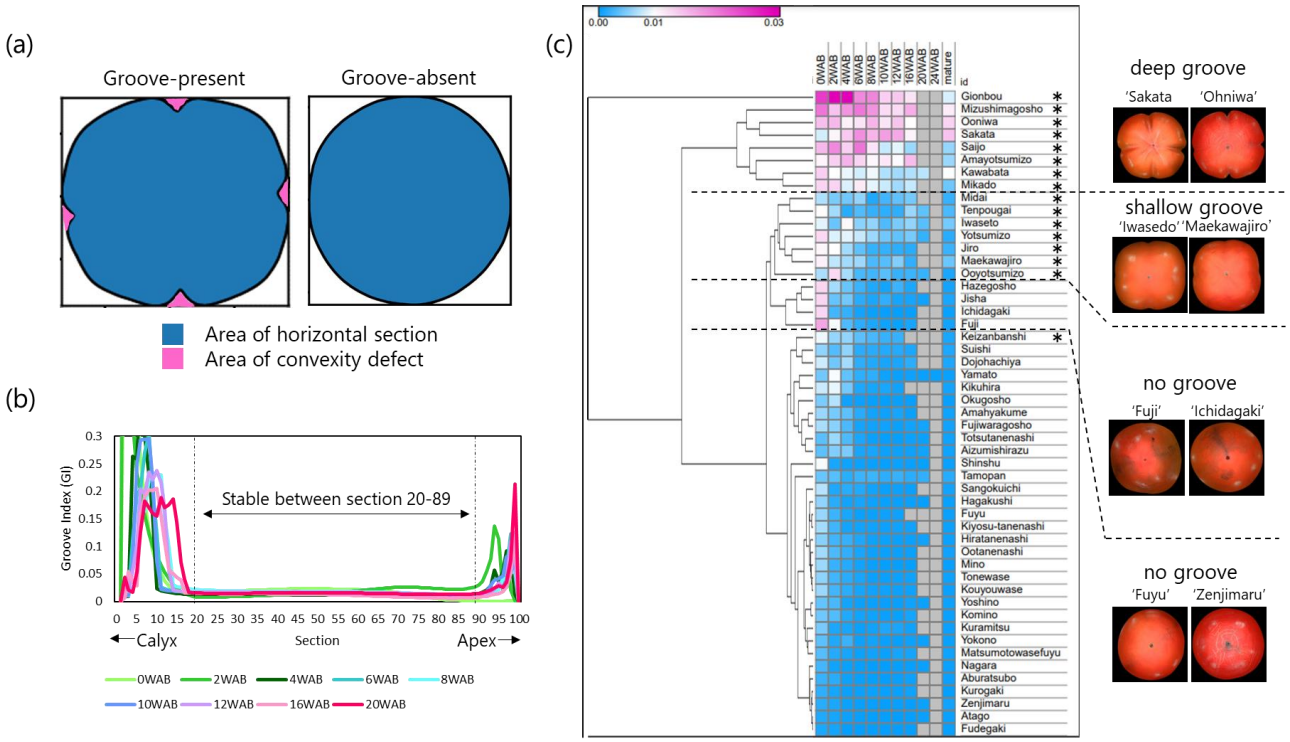


**Figure 2. Characterization of vertical groove development.** (a) Schematic of the measurement method used to determine groove index (GI). (b) Transition of GI in 'Ooniwa' throughout developmental stages. (c) Heatmap of the transition of GI#20-89, with asterisks indicating cultivars classified as having vertical grooves by Fruit Tree Experiment Station of Hiroshima Prefecture (1979) and visually verified when no recorded reference was available.

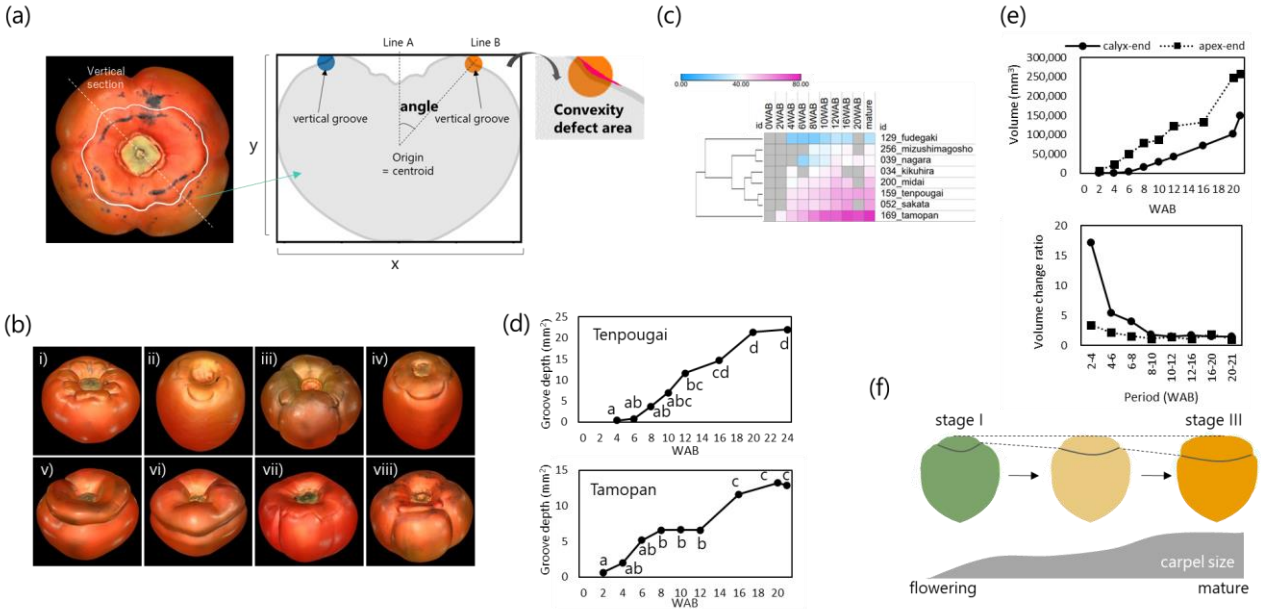


**Figure 3. Characterization of horizontal groove development.** (a) Schematic of the measurement method used to determine horizontal grooves. (b) 3D models of (i) 'Kikuhira,' (ii) 'Nagara,' (iii) 'Sakata,' (iv) 'Fudegaki,' (v) 'Tenpougai,' (vi) 'Tamopan,' (vii) 'Midai,' and (viii) 'Mizushimagosho.' (c) Heatmap of the transition of groove position (angle between line A and line B in Figure 3a). (d) Transition patterns of groove depth in 'Tenpougai' and 'Tamopan.' The black line indicates the horizontal groove depth. (e) Transition of volume and volume increase ratio in 'Tamopan.' (f) Proposed developmental model for horizontal grooves.

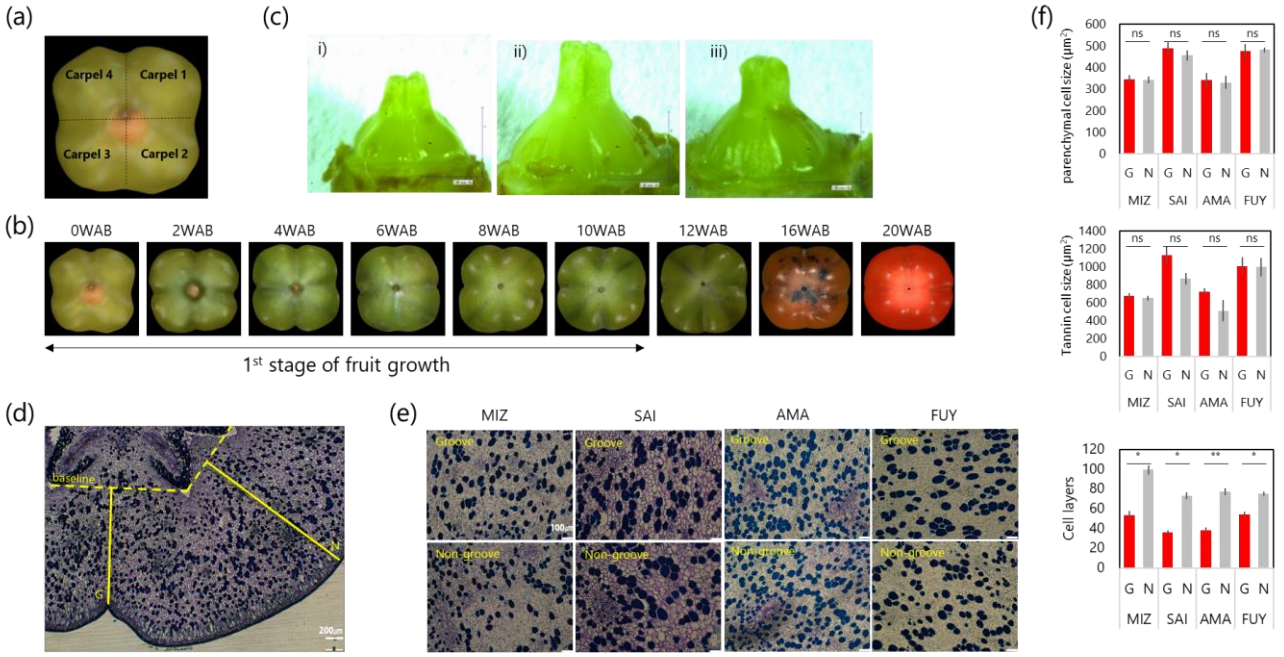


**Figure 4. Morphological characterization of groove tissue.** (a) 3D model of 'Gionbou' at anthesis showing grooves at the boundaries of the fused carpels. (b) Chronological change of groove development in 'Gionbou.' (c) Ovaries of (i) 'Amayotsumizo,' (ii) 'Mizushimagosho,' and (iii) 'Fuyuu' at three weeks before anthesis (23 April 2022). Grooving lines were observed in (i) and (ii), but not in (iii). (d) Measurement of cell number and area in the grooved and non-grooved zones using baselines set at the tip of developing seeds. (e) Microscopy analysis performed on grooved and non-grooved zones for four cultivars. MIZ, SAI, AMA, and FUY represent 'Mizushimagosho,' 'Saijou,' 'Amayotsumizo,' and 'Fuyuu,' respectively. (f) Comparison of parenchyma cell size, tannin cell size, and cell layers measured in each zone (grooved, G, and non-grooved, N) in four cultivars. Single and double asterisks indicate significant differences at $p < 0.05$ and $p < 0.01$, respectively.

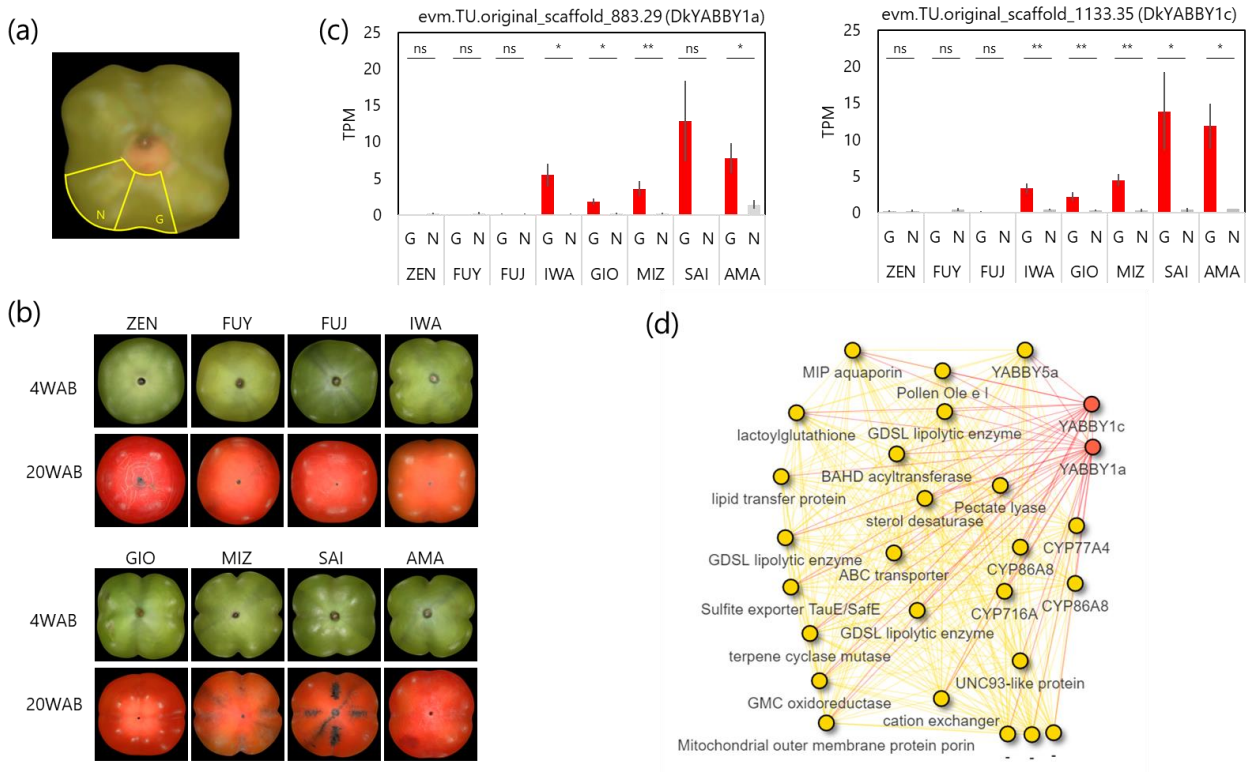


**Figure 5. Transcriptome analysis of vertical groove development.** (a) Grooved (G) and non-grooved (N) zones from which RNA was extracted. (b) Vertical groove depths at 4 and 20 WAB. (c) Expression patterns of *DkYABBY1a* and *DkYABBY1c*. (d) Gene co-expression network for *DkYABBY1a*/*1c*. The full network of this module is presented in Supplementary Figure S8. ZEN, FUY, FUJ, IWA, GIO, MIZ, SAI, and AMA represent 'Zenjimaru,' 'Fuyuu,' 'Fuji,' 'Iwasedo,' 'Gionbou,' 'Mizushimagosho,' 'Saijou,' and 'Amayotsumizo,' respectively.

**Table 1. Cultivars used in this study.**

| No. | Cultivar | Vertical groove | Horizontal groove | Determining timing (WAB) | | | | |
|---|---|---|---|---|---|---|---|---|
| | | | | GI#20-89 | Ro#20-89 | L/W | Horizontal groove position | Horizontal groove depth |
| 1 | Zenjimaru | | | 2 | 2 | 12 | | |
| 2 | Hazegosho | | | 2 | 6 | 8 | | |
| 3 | Maekawajiro | * | | 2 | 2 | 4 | | |
| 4 | Kurogaki | | | 4 | 4 | 4 | | |
| 5 | Aburatsubo | | | 4 | 8 | at maturity | | |
| 6 | Amayotsumizo | * | | 6 | 4 | 8 | | |
| 7 | Aizumishirazu | | | 6 | 6 | 8 | | |
| 8 | Fujiwaragosho | | | 4 | 4 | 4 | | |
| 9 | Kikuhira | | * | 4 | 0 | 4 | 4 | |
| 10 | Koyowase | | | 4 | 6 | 4 | | |
| 11 | Nagara | | * | 2 | 8 | at maturity | 12 | |
| 12 | Matsumotowasefuyuu | | | 2 | 4 | 2 | | |
| 13 | Totsutanenashi | | | 6 | 6 | 6 | | |
| 14 | Shinshuu | | | 2 | 6 | 20 | | |
| 15 | Sakata | * | * | 0 | 0 | 8 | 12 | |
| 16 | Tonewase | | | 4 | 0 | 6 | | |
| 17 | Atago | | | 4 | 6 | 4 | | |
| 18 | Gionbou | * | | 6 | 4 | 8 | | |
| 19 | Kiyosu-tanenashi | | | 4 | 10 | 6 | | |
| 20 | Ooyotsumizo | * | | 6 | 4 | 4 | | |
| 21 | Jisha | | | 6 | 4 | 8 | | |
| 22 | Ichidagaki | | | 2 | 8 | 8 | | |
| 23 | Saijou | * | | 8 | 10 | at maturity | | |
| 24 | Dojohachiya | | | 6 | 0 | 6 | | |
| 25 | Ootanenashi | | | 4 | 0 | 4 | | |
| 26 | Yokono | | | 2 | 4 | 8 | | |
| 27 | Fuji | | | 4 | 4 | 10 | | |
| 28 | Jirou | * | | 4 | 4 | 0 | | |
| 29 | Yamato | | | 6 | 10 | 12 | | |
| 30 | Fudegaki | | * | 4 | 4 | at maturity | 10 | |
| 31 | Komino | | | 4 | 6 | 4 | | |
| 32 | Amahyakume | | | 6 | 16 | 16 | | |
| 33 | Okugosho | | | 4 | 6 | 10 | | |
| 34 | Mino | | | 2 | 6 | 10 | | |
| 35 | Yoshino | | | 4 | 4 | 4 | | |
| 36 | Yotsumizo | * | | 8 | 2 | 2 | | |
| 37 | Tenpougai | * | * | 2 | 0 | 4 | 10 | 16 |
| 38 | Hiratanenashi | | | 6 | 2 | 4 | | |
| 39 | Tamopan | | * | 4 | 0 | 0 | at maturity | 16 |
| 40 | Fuyuu | | | 4 | 8 | 4 | | |
| 41 | Iwasedo | * | | 6 | 0 | 4 | | |
| 42 | Midai | * | * | 0 | 4 | 4 | 10 | |
| 43 | Hagakushi | | | 2 | 10 | 10 | | |
| 44 | Sangokuichi | | | 2 | 0 | 8 | | |
| 45 | Kuramitsu | | | 2 | 0 | 10 | | |
| 46 | Mizugaki/suishi | | | 6 | 0 | 8 | | |
| 47 | Ooniwa | * | | 0 | 0 | 8 | | |
| 48 | Kawabata | * | | 0 | 0 | 20 | | |
| 49 | Keizanbanshi | * | | 2 | 4 | 2 | | |
| 50 | Mikado | * | | 8 | 4 | 4 | | |
| 51 | Mizushimagosho | * | * | 8 | 8 | 4 | 8 | |

Asterisks indicates the presence of vertical or horizontal groove.

583 **Table 2. Top 20 genes based on the log2 fold change between grooved and non-grooved zones.**

| gene | log2fold (G/N) | q.value | Best Hit Arabidopsis gene model | description |
|---|---|---|---|---|
| evm.model.original_scaffold_841.12 | 1.05 | 5.77E-21 | AT4G03210.1 | xyloglucan endotransglucosylase/hydrolase |
| evm.model.original_scaffold_495.37 | -0.91 | 4.22E-19 | AT2G22540.1 | SVP |
| evm.model.original_scaffold_1133.35 | 3.80 | 2.22E-16 | AT2G45190.1 | YABBY |
| evm.model.fragScaff_scaffold_27.108 | 2.72 | 8.82E-16 | AT5G42180.1 | Peroxidase superfamily protein |
| evm.model.fragScaff_scaffold_16.567 | 3.77 | 8.18E-15 | AT5G36110.1 | cytochrome P450 family |
| evm.model.fragScaff_scaffold_101.67 | 3.14 | 5.40E-14 | AT1G71380.1 | Endoglucanase |
| evm.model.original_scaffold_883.29 | 3.96 | 5.40E-14 | AT2G45190.1 | YABBY |
| evm.model.original_scaffold_985.51 | 3.69 | 6.91E-14 | AT5G04660.1 | cytochrome P450 family |
| evm.model.fragScaff_scaffold_113.266 | 3.43 | 2.87E-13 | AT2G27385.1 | Pollen Ole e 1 allergen and extensin family protein |
| evm.model.fragScaff_scaffold_27.191 | 3.62 | 2.87E-13 | AT1G15380.1 | Glyoxalase |
| evm.model.fragScaff_scaffold_107.390 | 2.29 | 3.79E-13 | AT2G36380.1 | ABC transporter superfamily |
| evm.model.fragScaff_scaffold_45.92 | 3.82 | 4.16E-13 | AT1G15360.1 | Ethylene-responsive transcription factor WIN1-like |
| evm.model.original_scaffold_808.12 | 2.92 | 1.29E-12 | AT2G46770.1 | NAC domain-containing protein |
| evm.model.fragScaff_scaffold_83.149 | 3.72 | 1.33E-12 | AT2G40370.1 | Lignin degradation and detoxification of lignin-derived products |
| evm.model.original_scaffold_1962.72 | 3.65 | 3.22E-12 | AT4G28780.1 | GDSL lipolytic enzyme family |
| evm.model.fragScaff_scaffold_27.231 | 1.61 | 6.95E-12 | AT5G66390.1 | peroxidase |
| evm.model.original_scaffold_171.683 | 3.61 | 6.95E-12 | AT1G29670.2 | GDSL lipolytic enzyme family |
| evm.model.original_scaffold_1962.118 | 1.73 | 1.58E-11 | AT1G04040.1 | acid phosphatase |
| evm.model.fragScaff_scaffold_16.447 | 2.93 | 3.52E-11 | AT2G37170.2 | MIP aquaporin family |
| evm.model.fragScaff_scaffold_113.264 | 3.78 | 3.85E-11 | AT5G54160.1 | Cation-independent O- methyltransferase family |

584

585

586 **Table 3. GO enrichment analysis for DEGs**

| GO ID | Term | Annotated gene count | gene count in the cluster | Expected count | q-value |
|---|---|---|---|---|---|
| GO:0009834 | plant-type secondary cell wall biogenesis | 24 | 67 | 4.13 | 4.61E-07 |
| GO:0009699 | phenylpropanoid biosynthetic process | 26 | 90 | 5.55 | 1.18E-05 |
| GO:0009698 | phenylpropanoid metabolic process | 27 | 101 | 6.23 | 2.88E-05 |
| GO:0042335 | cuticle development | 15 | 37 | 2.28 | 5.85E-05 |
| GO:0042546 | cell wall biogenesis | 37 | 191 | 11.77 | 2.19E-04 |
| GO:0009809 | lignin biosynthetic process | 14 | 38 | 2.34 | 6.37E-04 |
| GO:0048046 | apoplast | 42 | 261 | 16.09 | 8.98E-04 |
| GO:0045491 | xylan metabolic process | 16 | 53 | 3.27 | 1.16E-03 |
| GO:0005618 | cell wall | 72 | 550 | 33.90 | 1.16E-03 |
| GO:0010383 | cell wall polysaccharide metabolic process | 22 | 93 | 5.73 | 1.16E-03 |
| GO:0030312 | external encapsulating structure | 72 | 552 | 34.03 | 1.16E-03 |
| GO:0010143 | cutin biosynthetic process | 11 | 26 | 1.60 | 1.16E-03 |
| GO:0009808 | lignin metabolic process | 14 | 42 | 2.59 | 1.16E-03 |
| GO:0009832 | plant-type cell wall biogenesis | 30 | 153 | 9.43 | 1.16E-03 |
| GO:0010410 | hemicellulose metabolic process | 18 | 68 | 4.19 | 1.23E-03 |
| GO:0044038 | cell wall macromolecule biosynthetic process | 17 | 63 | 3.88 | 1.46E-03 |
| GO:0070589 | cellular component macromolecule biosynthetic process | 17 | 63 | 3.88 | 1.46E-03 |
| GO:0071554 | cell wall organization or biogenesis | 57 | 407 | 25.09 | 2.71E-03 |
| GO:0071669 | plant-type cell wall organization or biogenesis | 42 | 267 | 16.46 | 2.90E-03 |
| GO:0044036 | cell wall macromolecule metabolic process | 25 | 125 | 7.71 | 3.14E-03 |
| GO:0009505 | plant-type cell wall | 42 | 276 | 17.01 | 3.46E-03 |
| GO:0044550 | secondary metabolite biosynthetic process | 33 | 190 | 11.71 | 3.55E-03 |
| GO:0045492 | xylan biosynthetic process | 13 | 43 | 2.65 | 3.70E-03 |
| GO:0070592 | cell wall polysaccharide biosynthetic process | 16 | 62 | 3.82 | 3.86E-03 |
| GO:0010025 | wax biosynthetic process | 11 | 31 | 1.91 | 5.67E-03 |
| GO:0006649 | phospholipid transfer to membrane | 5 | 8 | 0.49 | 6.55E-03 |
| GO:0010166 | wax metabolic process | 11 | 35 | 2.16 | 1.61E-02 |
| GO:0019748 | secondary metabolic process | 39 | 266 | 16.40 | 1.95E-02 |
| GO:1901570 | fatty acid derivative biosynthetic process | 11 | 37 | 2.28 | 3.02E-02 |
| GO:1901957 | regulation of cutin biosynthetic process | 7 | 17 | 1.05 | 3.02E-02 |
| GO:0016841 | ammonia-lyase activity | 6 | 12 | 0.74 | 4.20E-02 |
| GO:0005576 | extracellular region | 53 | 440 | 27.12 | 4.76E-02 |
| GO:0005875 | microtubule associated complex | 19 | 99 | 6.10 | 5.36E-02 |
| GO:0000786 | nucleosome | 5 | 11 | 0.68 | 5.36E-02 |
| GO:0045548 | phenylalanine ammonia-lyase activity | 4 | 5 | 0.31 | 6.54E-02 |
| GO:0010090 | trichome morphogenesis | 16 | 78 | 4.81 | 6.54E-02 |
| GO:1901568 | fatty acid derivative metabolic process | 13 | 55 | 3.39 | 6.54E-02 |
| GO:0005874 | microtubule | 19 | 101 | 6.23 | 7.20E-02 |
| GO:0010158 | abaxial cell fate specification | 5 | 9 | 0.55 | 7.56E-02 |

587